

Fracture toughening and toughness asymmetry induced by flexoelectricity

Amir Abdollahi,^{1,2} Christian Peco,¹ Daniel Millán,¹ Marino Arroyo,¹ Gustau Catalan,^{2,3} and Irene Arias^{1,*}

¹Laboratori de Càlcul Numèric (LaCàN), Universitat Politècnica de Catalunya (UPC), Campus Nord UPC-C2, E-08034 Barcelona, Spain

²ICN2-Institut Català de Nanociència i Nanotecnologia, Bellaterra 08193, Barcelona, Spain

³ICREA-Institut Català de Recerca i Estudis Avançats, Barcelona, Spain

(Received 2 December 2014; revised manuscript received 16 August 2015; published 8 September 2015)

Cracks generate the largest strain gradients that any material can withstand. Flexoelectricity (coupling between strain gradient and polarization) must therefore play an important role in fracture physics. Here we use a self-consistent continuum model to evidence two consequences of flexoelectricity in fracture: the resistance to fracture increases as structural size decreases, and it becomes asymmetric with respect to the sign of polarization. The latter phenomenon manifests itself in a range of intermediate sizes where piezo- and flexoelectricity compete. In BaTiO₃ at room temperature, this range spans from 0.1 to 50 nm, a typical thickness range for epitaxial ferroelectric thin films.

DOI: [10.1103/PhysRevB.92.094101](https://doi.org/10.1103/PhysRevB.92.094101)

PACS number(s): 77.65.-j, 62.20.mt, 62.25.Mn

The best known and most technologically exploited electromechanical coupling mechanism in solids is piezoelectricity, by which electric polarization is generated by strain, or conversely strain is generated by an applied electric field. Flexoelectricity is a different electromechanical coupling mechanism, whereby polarization couples to spatial variations of the strain field (strain gradients). Flexoelectricity is a more widespread property than piezoelectricity—it is, in fact, a universal property of all insulators [1–3], and it is particularly strong in materials with high dielectric constants such as ferroelectrics [4–9].

Because of the size dependence of strain gradients, flexoelectricity is most conspicuous at the nanoscale. At these scales, large strain gradients can be achieved without rupture, leading to large flexoelectric effects in samples such as thin films [10] and near nano-inclusions [11,12]. Recent nanoindentation experiments on ferroelectrics have shown a strong size-dependent stiffening [13,14] and electric-field-dependent elastic modulus [15], attributed to flexoelectricity caused by the highly inhomogeneous strain field produced by the nanoindenter. Flexoelectric sensors based on ferroelectrics have been proposed to detect localized damage where strain gradients are prominent [16]. These results highlight the effect of flexoelectricity on mechanical properties, and suggest that flexoelectricity may play an important and hitherto overlooked role in fracture physics.

The ultimate strain gradient that any material can withstand is that which exists around a crack tip: the material just before the crack apex is, by definition, on the verge of rupture, and hence under the maximum deformation it can stand, while the distance over which this strain is released tends towards the atomic scale at the apex. Cracks are therefore a natural ground where to search for flexoelectric effects.

In this paper, we analyze the fracture of ferroelectrics using a self-consistent model of flexoelectricity [17,18]. Macroscopic experiments [19,20] have already shown that the resistance to cracking depends on the *direction* of polarization, in agreement with theoretical models, coupling fracture and

ferroelectricity [21,22]. Here, we find that, in the presence of flexoelectricity, the resistance to fracture significantly increases (fracture toughening) in a size-dependent manner, and moreover that this toughening is asymmetric with respect to the *sign* of the polarization. The latter observation is the most far-reaching result of this paper, as it challenges the theory of mechanical properties, which predicates that in the absence of flexoelectricity all mechanical properties of all materials—including ferroelectrics—are symmetric with respect to space inversion.

To examine the role of flexoelectricity on fracture physics of polar materials, we consider a linear continuum theory of piezoelectricity with poling [23], augmented with flexoelectricity [17]. We discuss later the quantitative limitations of this simple but transparent model. The electrical enthalpy density of a poled piezoelectric solid possessing piezoelectricity and flexoelectricity can be written as

$$\begin{aligned} \mathcal{H}(\varepsilon_{ij}, E_i, \nabla_l \varepsilon_{jk}) &= \frac{1}{2} \mathbb{C}_{ijkl} \varepsilon_{ij} \varepsilon_{kl} - e_{ikl} E_i \varepsilon_{kl} - \mu_{ijkl} E_i \nabla_l \varepsilon_{jk} \\ &\quad + \frac{1}{2} g_{ijklmn} \nabla_k \varepsilon_{ij} \nabla_n \varepsilon_{lm} - \frac{1}{2} k_{ij} E_i E_j, \end{aligned} \quad (1)$$

where \mathbf{E} is the electric field, defined as $E_i = -\nabla_i \phi$, ϕ being the electric potential. The first term is the elastic potential, where \mathbb{C} is the fourth-rank tensor of elastic moduli. The piezoelectric coupling between strain and electric field is through the second term via the third-rank tensor of piezoelectricity \mathbf{e} . In this formulation, the remanent state of the piezoelectric material has been taken as the reference configuration, and the poling of the piezoelectric material is implicitly encoded in the symmetry of the piezoelectric tensor \mathbf{e} [23]. The last term is the electrostatic potential, where \mathbf{k} is the second-rank dielectric tensor. The flexoelectric coupling between the gradient of strain $\nabla \varepsilon$ and the electric field is through the third term, where the fourth-rank flexoelectric tensor $\boldsymbol{\mu}$ describes both direct and converse flexoelectric effects [24,25]. The fourth term is the strain gradient elastic potential, \mathbf{g} being the sixth-rank strain gradient elasticity tensor. This term is usually discarded, but it is important in the presence of strong elastic gradients, and it guarantees the thermodynamic stability of the model in the presence of flexoelectricity [11,25–27]. Alternatively, the

*irene.arias@upc.edu

thermodynamic stability can be maintained by including the correlation energy (square of the polarization gradient) in the thermodynamic potential [1,26,28]. The electric displacement \mathbf{D} can be derived from Eq. (1) by differentiating with respect to $-\mathbf{E}$. Since $\mathbf{D} = \varepsilon_0 \mathbf{E} + \mathbf{P}$, where \mathbf{P} is the electric polarization and ε_0 is the permittivity of free space, and introducing the dielectric susceptibility $\chi_{ij} = k_{ij} - \varepsilon_0 \delta_{ij}$, we obtain the constitutive relation for polarization as

$$P_i = \chi_{ij} E_j + e_{ikl} \varepsilon_{kl} + \mu_{ijkl} \nabla_l \varepsilon_{jk}, \quad (2)$$

which includes dielectric, piezoelectric, and flexoelectric contributions [1,29].

Defining a usual stress tensor $\hat{\sigma}$ and a higher-order (hyper) stress $\tilde{\sigma}$ arising from flexoelectricity

$$\hat{\sigma}_{ij} = \frac{\partial \mathcal{H}}{\partial \varepsilon_{ij}}, \quad \tilde{\sigma}_{ijk} = \frac{\partial \mathcal{H}}{\partial \nabla_k \varepsilon_{ij}}, \quad (3)$$

the constitutive equation for the mechanical (Cauchy) stress σ emerging from the theory can be written as

$$\begin{aligned} \sigma_{ij} &= \hat{\sigma}_{ij} - \tilde{\sigma}_{ijk,k} \\ &= \mathbb{C}_{ijkl} \varepsilon_{kl} - e_{kij} E_k + \mu_{lijk} \nabla_k E_l - g_{ijklmn} \varepsilon_{lm,nk}, \end{aligned} \quad (4)$$

where the converse flexoelectric effect is through the third term, $\nabla \mathbf{E}$ being the electric field gradient. This contribution to Hook's law has been included in the constitutive equations of flexoelectric materials [30], as well as electromechanically coupled mixed ionic-electronic conductors [31].

In this model the essential and natural electrical boundary conditions are identical to those of electrostatics

$$\phi = \bar{\phi} \quad \text{on} \quad \Gamma_\phi, \quad (5)$$

$$D_i n_i = -\omega \quad \text{on} \quad \Gamma_D, \quad (6)$$

where $\bar{\phi}$ and ω are the prescribed electric potential and surface charge density, n_i is the outer unit normal to the boundary of the domain Ω , and Γ_ϕ and Γ_D are disjoint parts of the boundary of the domain, $\partial\Omega$, whose union is the whole boundary, $\Gamma_\phi \cup \Gamma_D = \partial\Omega$. As for the mechanical boundary conditions, either displacement or traction needs to be specified:

$$u_i = \bar{u}_i \quad \text{on} \quad \Gamma_u, \quad (7)$$

$$\begin{aligned} t_k &= n_j (\hat{\sigma}_{jk} - \tilde{\sigma}_{ijk,i}) - V_j (n_i \tilde{\sigma}_{ijk}) - (V_p n_p) n_i n_j \tilde{\sigma}_{ijk} \\ &= \bar{t}_k \quad \text{on} \quad \Gamma_t, \end{aligned} \quad (8)$$

where \bar{u}_i and \bar{t}_k are the prescribed mechanical displacements and tractions, $V_j = \partial_j - n_j V^n$ is the surface gradient operator, $V^n = n_k \partial_k$ is the normal gradient operator, and $\Gamma_u \cup \Gamma_t = \partial\Omega$. It is clear that the traction boundary condition in Eq. (8) is affected by the higher-order stresses. In addition to these boundary conditions, the strain gradients result in other types

of boundary conditions [27,32]

$$u_{i,j} n_j = \bar{v}_i \quad \text{on} \quad \Gamma_v, \quad (9)$$

$$n_i n_j \tilde{\sigma}_{ijk} = \bar{r}_k \quad \text{on} \quad \Gamma_r, \quad (10)$$

where \bar{v} is the prescribed normal derivative of displacement, \bar{r}_k is the higher-order traction, and $\Gamma_v \cup \Gamma_r = \partial\Omega$. Here, we assume $\Gamma_r = \partial\Omega$ and natural boundary conditions, $\bar{\mathbf{r}} = \mathbf{0}$.

In the absence of surface charges, the total electromechanical enthalpy is

$$H = \int_{\Omega} \mathcal{H} d\Omega - \int_{\Gamma_t} \bar{t}_i u_i dS, \quad (11)$$

where $\bar{\mathbf{t}}$ are the mechanical tractions applied on the boundary. The self-consistent governing equations in weak form for the electromechanical boundary value problem follow from making the enthalpy stationary with respect to the displacement and electric potential fields [17]. Numerically, we deal with the fourth-order nature of the partial differential equations by approximating displacements and electric potential using a mesh-free method with smooth basis functions [33].

To evaluate the role of flexoelectricity on the fracture of ferroelectrics, we compute energy release rates in a poled specimen. In Griffith's theory, fracture occurs when the energy release rate G reaches the energetic fracture toughness of the material G_c . Therefore, a decrease in G due to the electromechanical coupling is interpreted as a toughening effect on the material [34,35]. The energy-release rate G is defined as the reduction in the potential energy of the cracked body per unit increase in the crack length a (in two dimensions). Considering two cracked plane specimens with the same material, configuration, loading and boundary conditions, and cracks of slightly different length Δa , the energy release rate can be computed as $G = [H(a) - H(a + \Delta a)]/\Delta a$, where H is given in Eq. (11).

We consider two pre-cracked beams, with pre-crack lengths of $a = h/4$ and $a = h/4 + h/1000$ ($\Delta a = h/1000$), in a four-point bending configuration as shown in Fig. 1(a), with the material properties of barium titanate (BaTiO_3) [36] and poled along the x_2 axis. We consider both the longitudinal and transversal flexoelectric coefficients μ_{11} and μ_{12} . Given that there is not yet a universal consensus regarding the size, or even the sign, of these coefficients for any material [2], we consider three cases C1: $\mu_{11} = \mu_{12}$, C2: $\mu_{12} = -10\mu_{11}$, and C3: $\mu_{11} = 2\mu_{12}$, where the latter two limiting cases are chosen according to reported values for ferroelectrics [7,37,38]. The magnitude of these coefficients is chosen as $\mu = \chi f$, where f is the flexocoupling coefficient and the dielectric susceptibility of BaTiO_3 at room temperature is $\chi_{11} = 36 \text{ nC (V m)}^{-1}$ along the a axis and $\chi_{33} = 1.7 \text{ nC (V m)}^{-1}$ along the c axis [39]. The value of f has been estimated to be of the order of 1–10 V for simple ionic solids [2]. We choose an average value of $f = 10 \text{ V}$, as measured on single crystals [40]. Although surface piezoelectricity is theoretically expected to contribute to the total flexoelectric coefficient [41], we do not incorporate it as a separate term since (i) the actual thickness and piezoelectric coefficient of the surface have not yet been characterized for any material and (ii) the effect of surface piezoelectricity is contained within the effective flexoelectric

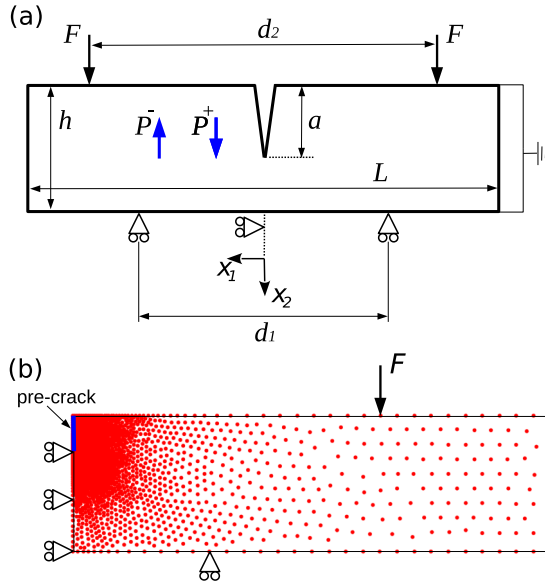


FIG. 1. (Color online) (a) Four-point bending setup with dimensions $L = 7h = 3.5d_1 = 1.5d_2$. The specimen is poled along the positive (P^+) and negative (P^-) x_2 directions, i.e., parallel and antiparallel to the crack, respectively. The top and bottom sides are connected to the ground. (b) Computational node set.

coefficient [41,42]. The parameter $g = 1.4 \times 10^{-9}$ N is chosen to satisfy the stability condition for the flexoelectric equations [27], in the order chosen in [25].

The energy-release rate is obtained as a function of the beam thickness h with the poling direction parallel (positive) and antiparallel (negative) to the pre-crack; see Fig. 1(a). To screen the surface depolarization field, we assume that the top and bottom sides of the beam are connected to the ground; i.e., the electric potential is fixed to zero, while other sides are charge-free. The aspect ratio of the beam is fixed to $L/h = 7$, L being the length of the beam. For symmetry reasons, only the right half of the beam is analyzed. A nonuniform node distribution is considered for the model discretization, with higher concentration of nodes around the crack tip, as shown in Fig. 1(b). A point load $F = 9 \times 10^4 \sqrt{h}$ N $m^{-1/2}$ is considered to supply sufficient energy for fracture at different length scales; i.e., the calculated energy release rates are on the order of the energetic fracture toughness of BaTiO₃, $G_c = 2$ (J m^{-2}) [21].

The flexoelectric model adopted here has several intrinsic length scales, in particular that given by the balance between piezo- and flexoelectricity, $\ell_1 = \mu/e$, and that resulting from the competition between usual and strain-gradient elasticity, $\ell_2 = \sqrt{g/Y}$, where Y is the Young's modulus. With our parameters, $Y = 160$ GPa and the piezoelectric coefficient $e_{33} = 5.5$ C m^{-2} for BaTiO₃ [36], we find $\ell_1 \approx 6$ nm and $\ell_2 \approx 0.1$ nm, the latter in agreement with [43]. We examine next how these length scales manifest themselves around a crack tip. Figure 2 shows the relative weight of the different terms in the electrical enthalpy density in Eq. (1) as we approach the crack tip along the symmetry plane shown in Fig. 1(b). It can be observed that, as estimated by ℓ_1 , the flexoelectric contribution dominates the piezoelectric contribution below

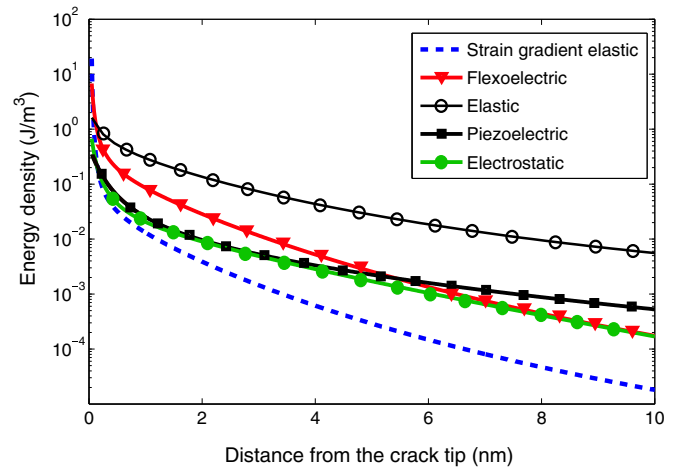


FIG. 2. (Color online) Relative weight of the different terms in the electrical enthalpy density in Eq. (1) as a function of the distance from the crack tip.

around 6 nm. Similarly, the strain gradient elastic term only becomes relevant and larger than the usual elastic term at very small scales comparable to ℓ_2 . This analysis suggests that, since ℓ_2 is much smaller than ℓ_1 and than structural size, it does not play a quantitative role in our calculations, other than guaranteeing thermodynamical stability. Our numerical experiments suggest that both of these length scales, ℓ_1 and ℓ_2 , need to be resolved with a fine node distribution near the crack tip for stable numerical solutions.

Figure 3(a) presents the energy release rate G as a function of the beam thickness h for the poled piezoelectric beam with and without considering flexoelectricity. As expected, without the flexoelectric effect, the energy release rate is independent both of the size of the beam and the poling direction; see Fig. 3(a). By introducing flexoelectricity, we observe two effects: (1) the energy release rate decreases with the beam thickness, i.e., the thinner the beam, the tougher, and (2) this fracture toughness enhancement is sensitive to the poling direction, which we term fracture toughness asymmetry. For instance, a 78% reduction in energy release rate is observed for the parallel (positive) poling direction in the C2 case for a thickness of 2.4 nm, corresponding to the thinnest BaTiO₃ film retaining ferroelectricity [44]. While for BaTiO₃ smaller sizes are not physically meaningful, we report results corresponding to thicknesses below 2.4 nm to examine the general features of fracture physics in the presence of flexoelectricity, which may be relevant for other materials that preserve piezoelectricity down to lower film thickness such as BaZrO₃ [45] and PbTiO₃ [46], or for materials with larger length scale ℓ_1 than BaTiO₃. We also note that at very small scales, our continuum model may become questionable due to lattice rearrangements, such as crack-tip blunting as a result of dislocation emission.

To understand the origin of the fracture toughness enhancement, we plot maps of polarization magnitude for different beam thicknesses, shown in Fig. 3(b) for the positively poled piezoelectric beam with flexoelectricity in the C2 case. Since the electric field is induced by the flexo- and piezoelectric effects, we can graphically represent the polarization pattern by focusing on the dielectric polarization $\mathbf{P}_e = \chi \mathbf{E}$. As the beam

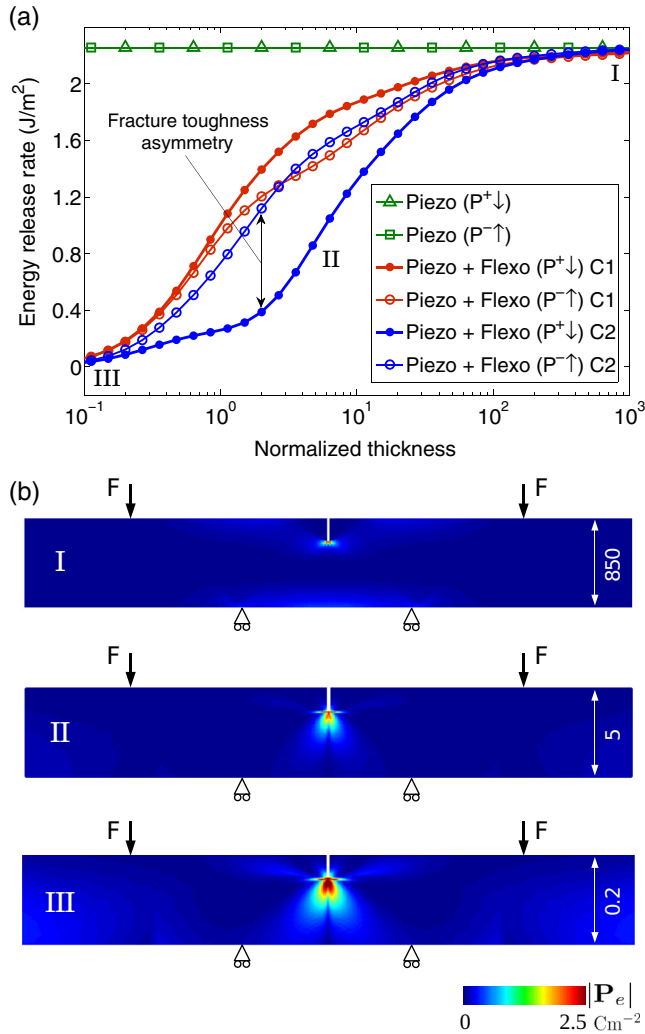


FIG. 3. (Color online) (a) Energy release rate as a function of the normalized thickness of the poled piezoelectric beam with and without flexoelectricity. The results are obtained considering the material is poled parallel (+) and antiparallel (−) to the crack. Two cases of the flexoelectric coefficients (C1: $\mu_{11} = \mu_{12}$ and C2: $\mu_{12} = -10\mu_{11}$) are considered for the piezoelectric beam with flexoelectricity. (b) Distribution of the polarization magnitude $|\mathbf{P}_e|$ for three different thicknesses (marked as I–III above) considering the positively poled piezoelectric beam with flexoelectricity in the C2 case. The beam thickness is normalized by a factor of $\ell_1/6$ (1 nm for BaTiO₃).

thickness decreases, the relative size of the flexoelectrically polarized region around the crack tip increases. A similar and smaller effect is also observed for the negatively poled piezoelectric beam and for the other two cases C1 and C3 (not shown). In the absence of flexoelectricity, we obtain a polarization magnitude map similar to that in Fig. 3(b), panel I, irrespective of the beam thickness.

The response of the beam with the flexoelectric effect is also sensitive to the poling direction. Figure 3(a) shows that the energy release rate of the beam (C2) with the positive poling direction is lower than that with negative poling direction; i.e., the beam poled parallel to the crack is tougher. This direction is reversed in the C1 and C3 cases. Figure 4 presents the fracture

toughness asymmetry obtained as the absolute percentage difference between the energy release rates of the negatively and positively poled beams with flexoelectricity, as a function of the beam thickness. The insets show the polarization field in a small area around the crack tip for three different beam thicknesses for both the negatively and positively poled material in the C2 case. A significant asymmetry is observed in a wide range of beam thickness (spanning over one order of magnitude).

For thick beams, the response is dominated by piezoelectricity, Fig. 4, inset (I \pm), while for thin beams, the response is mainly due to flexoelectricity, Fig. 4, inset (III \pm). The polarization fields induced by piezoelectricity in Fig. 4, insets (I−) and (I+), are antisymmetric with respect to changing the poling sign; i.e., they are identical in magnitude but have reverse direction. As shown in Fig. 3(a), this sign reversal does not affect the material toughness. Turning now to the small-scale limit, the flexoelectric-induced fields are symmetric with respect to changing the poling sign; i.e., they do not depend on the poling direction, see Fig. 4, insets (III−) and (III+), since they are induced by strain gradients. Therefore, if either piezo- or flexoelectricity dominates the response, reversing the poling direction of the material does not affect the fracture toughness. In contrast, for intermediate sizes, flexo- and piezoelectricity are comparable effects, and may therefore help or counteract each other; for a positively poled material, the piezo- and flexoelectric polarization fields point in the same direction in front of the crack and in the opposite direction in its wake, while this situation is reversed for a negatively poled material, resulting in a fundamentally different polarization pattern; see Fig. 4, insets (II−) and (II+). This explains the significant fracture toughness asymmetry at intermediate beam sizes, comparable to ℓ_1 .

For BaTiO₃ at room temperature, the range with significant fracture toughness asymmetry is between 0.1 nm and 50 nm approximately. This is a typical thickness range for epitaxial ferroelectric thin films. For the critical thickness 2.4 nm, the asymmetry reaches a considerable value of about 90% in the C2 case; such enormous toughness asymmetry should be observable via nanoindentation experiments in epitaxial films.

Domain switching makes the fracture response of ferroelectrics more complex [21,23,47,48]. As mentioned earlier, the present model is based on the linear theory of piezoelectricity in the absence of domain switching. However, in ferroelectric materials such as BaTiO₃ in the tetragonal phase, ferroelastic switching becomes favorable when the polarization is parallel to the crack. Ferroelastic switching is precluded in BaTiO₃ thin films epitaxially clamped onto substrates imposing compressive in-plane strain. Even then, a strong enough flexoelectric field can induce 180° switching of the material polarization, the so-called flexoelectric switching [1,2,10]. If switching occurs, it may lead to energy dissipation near the crack tip, consequently leading to stronger fracture toughness asymmetry.

The calculated size of the flexoelectrically induced polarization near the tip apex is huge: 2.5 C/m². This is 10 times larger than the actual ferroelectric polarization of BaTiO₃. This is of course the reason why in the low thickness limit the toughness is insensitive to the ferroelectric orientation. The size of the flexoelectric polarization is so large that

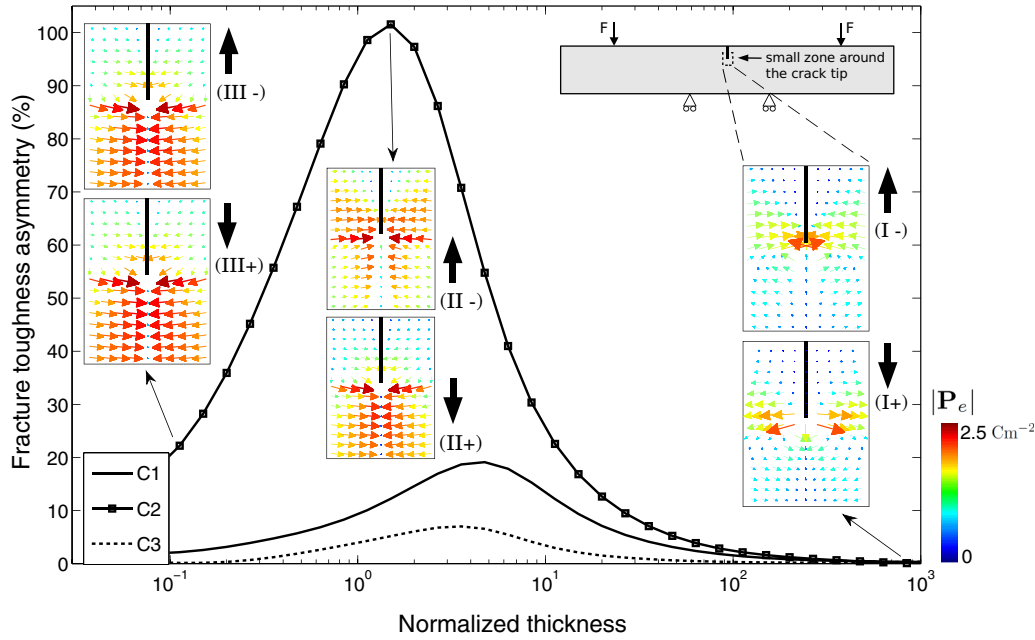


FIG. 4. (Color online) Fracture toughness asymmetry as a function of the normalized beam thickness. The asymmetry is obtained as the absolute percentage difference between the energy release rates of the negatively and positively poled piezoelectric beams with flexoelectricity, presented in Fig. 3 for two cases of the flexoelectric coefficients (C1: $\mu_{11} = \mu_{12}$ and C2: $\mu_{12} = -10\mu_{11}$), and the additional case C3: $\mu_{11} = 2\mu_{12}$. The insets show the distribution of the polarization P_e in a small zone around the crack tip at three different length scales for the negative (top) and positive (bottom) poling directions in the C2 case. The bold black line shows the position of the pre-crack and the bold black arrow indicates the poling direction of the beam. The beam thickness is normalized by a factor of $\ell_1/6$ (1 nm for BaTiO₃).

higher-order coupling terms should not be neglected [49,50]. The magnitude of these terms, however, is still unknown and we hope this discussion motivates more research into the measurement of higher-order flexoelectric coefficients. It has also been suggested that, because soft materials can withstand larger strain gradients, flexoelectricity is likely to play a significant role in this context [51,52], where fracture is significantly affected by elastic nonlinearity near the crack tip [53]. Thus, the inclusion of nonlinear effects is the natural next step in understanding the physics of fracture and flexoelectricity. It would be very interesting to corroborate our results with atomistic calculations, but unfortunately this is extremely challenging because the physical effects that we are reporting require spanning several orders of magnitude in size.

In summary, the flexoelectric effect leads to a significant enhancement in fracture toughness of BaTiO₃ at thicknesses below 50 nm. Importantly, at intermediate scales the fracture toughness is sensitive to the poling direction of the material

(parallel or antiparallel to the crack), which is not the case in the absence of flexoelectricity [21,22]. Flexoelectricity therefore fundamentally changes the symmetry of fracture physics: while crack propagation was hitherto thought to be invariant with respect to space inversion for all materials, the present work shows that this symmetry is broken in polar materials. This phenomenology can be understood in simple terms from the symmetry and size dependence of flexoelectricity. We predict that the toughness asymmetry could reach values as high as 100% for ultrathin epitaxial films of BaTiO₃.

The authors gratefully acknowledge the support of the Ministerio de Ciencia e Innovación (DPI2011-26589). G.C.'s research is supported by an ERC Starting Grant (Project No. 308023), by project FIS2013-48668 from the Ministerio de Ciencia e Innovación, and by the Severo Ochoa Excellence Award of ICN2.

[1] P. V. Yudin and A. K. Tagantsev, *Nanotechnology* **24**, 432001 (2013).
 [2] P. Zubko, G. Catalan, and A. K. Tagantsev, *Annu. Rev. Mater. Res.* **43**, 387 (2013).
 [3] T. D. Nguyen, S. Mao, Y.-W. Yeh, P. K. Purohit, and M. C. McAlpine, *Adv. Mater.* **25**, 946 (2013).
 [4] W. Ma and L. E. Cross, *Appl. Phys. Lett.* **81**, 3440 (2002).
 [5] W. Ma and L. E. Cross, *Appl. Phys. Lett.* **86**, 072905 (2005).
 [6] W. Ma and L. E. Cross, *Appl. Phys. Lett.* **88**, 232902 (2006).
 [7] P. Zubko, G. Catalan, A. Buckley, P. R. L. Welche, and J. F. Scott, *Phys. Rev. Lett.* **99**, 167601 (2007).
 [8] L. Shu, X. Wei, L. Jin, Y. Li, H. Wang, and X. Yao, *Appl. Phys. Lett.* **102**, 152904 (2013).
 [9] J. Narvaez and G. Catalan, *Appl. Phys. Lett.* **104**, 162903 (2014).
 [10] H. Lu, C. W. Bark, D. E. D. L. Ojos, J. Alcala, C. B. Eom, G. Catalan, and A. Gruverman, *Science* **336**, 59 (2012).
 [11] R. Maranganti, N. D. Sharma, and P. Sharma, *Phys. Rev. B* **74**, 014110 (2006).

- [12] N. D. Sharma, R. Maranganti, and P. Sharma, *J. Mech. Phys. Solids* **55**, 2328 (2007).
- [13] M. Gharbi, Z. H. Sun, P. Sharma, and K. White, *Appl. Phys. Lett.* **95**, 142901 (2009).
- [14] C. R. Robinson, K. W. White, and P. Sharma, *Appl. Phys. Lett.* **101**, 122901 (2012).
- [15] H. Zhou, Y. Pei, F. Li, H. Luo, and D. Fang, *Appl. Phys. Lett.* **104**, 061904 (2014).
- [16] W. Huang, X. Yan, S. R. Kwon, S. Zhang, F. G. Yuan, and X. Jiang, *Appl. Phys. Lett.* **101**, 252903 (2012).
- [17] A. Abdollahi, C. Peco, D. Millán, M. Arroyo, and I. Arias, *J. Appl. Phys.* **116**, 093502 (2014).
- [18] A. Abdollahi, D. Millán, C. Peco, M. Arroyo, and I. Arias, *Phys. Rev. B* **91**, 104103 (2015).
- [19] C. T. Sun and S. B. Park, *Ferroelectrics* **248**, 79 (2000).
- [20] G. A. Schneider, *Annu. Rev. Mater. Res.* **37**, 491 (2007).
- [21] A. Abdollahi and I. Arias, *Acta Mater.* **59**, 4733 (2011).
- [22] A. Abdollahi and I. Arias, *Model. Simul. Mater. Sci. Eng.* **19**, 074010 (2011).
- [23] A. Abdollahi and I. Arias, *J. Mech. Phys. Solids* **60**, 2100 (2012).
- [24] N. D. Sharma, C. M. Landis, and P. Sharma, *J. Appl. Phys.* **108**, 024304 (2010).
- [25] N. D. Sharma, C. Landis, and P. Sharma, *J. Appl. Phys.* **111**, 059901 (2012).
- [26] E. A. Eliseev, A. N. Morozovska, M. D. Glinchuk, and R. Blinc, *Phys. Rev. B* **79**, 165433 (2009).
- [27] S. Mao and P. K. Purohit, *J. Appl. Mech.* **81**, 081004 (2014).
- [28] P. V. Yudin, R. Ahluwalia, and A. K. Tagantsev, *Appl. Phys. Lett.* **104**, 082913 (2014).
- [29] S. M. Kogan, *Sov. Phys. Solid State* **5**, 2069 (1964).
- [30] L. E. Cross, *J. Mater. Sci.* **41**, 53 (2006).
- [31] A. N. Morozovska, E. A. Eliseev, A. K. Tagantsev, S. L. Bravina, L.-Q. Chen, and S. V. Kalinin, *Phys. Rev. B* **83**, 195313 (2011).
- [32] A. Yurkov, *JETP Lett.* **94**, 455 (2011).
- [33] M. Arroyo and M. Ortiz, *Int. J. Numer. Meth. Eng.* **65**, 2167 (2006).
- [34] R. M. McMeeking, *Eng. Fract. Mech.* **64**, 217 (1999).
- [35] W. Y. Li, R. M. McMeeking, and C. M. Landis, *Eur. J. Mech. A-Solids* **27**, 285 (2008).
- [36] Z. Li, S. K. Chan, M. H. Grimsditch, and E. S. Zouboulis, *J. Appl. Phys.* **70**, 7327 (1991).
- [37] R. Maranganti and P. Sharma, *Phys. Rev. B* **80**, 054109 (2009).
- [38] I. Ponomareva, A. K. Tagantsev, and L. Bellaiche, *Phys. Rev. B* **85**, 104101 (2012).
- [39] W. J. Merz, *Phys. Rev.* **76**, 1221 (1949).
- [40] J. Narvaez, S. Saremi, J. Hong, M. Stengel, and G. Catalan, *Phys. Rev. Lett.* **115**, 037601 (2015).
- [41] A. K. Tagantsev and A. S. Yurkov, *J. Appl. Phys.* **112**, 044103 (2012).
- [42] M. Stengel, *Phys. Rev. B* **90**, 201112 (2014).
- [43] R. Maranganti and P. Sharma, *Phys. Rev. Lett.* **98**, 195504 (2007).
- [44] J. Junquera and P. Ghosez, *Nature (London)* **422**, 506 (2003).
- [45] Y. Zhang, G.-P. Li, T. Shimada, J. Wang, and T. Kitamura, *Phys. Rev. B* **90**, 184107 (2014).
- [46] D. D. Fong, A. M. Kolpak, J. A. Eastman, S. K. Streiffer, P. H. Fuoss, G. B. Stephenson, C. Thompson, D. M. Kim, K. J. Choi, C. B. Eom, I. Grinberg, and A. M. Rappe, *Phys. Rev. Lett.* **96**, 127601 (2006).
- [47] Y. Jiang, D. Fang, and F. Li, *Appl. Phys. Lett.* **90**, 222907 (2007).
- [48] Y. Li and F. Li, *Scripta Mater.* **67**, 601 (2012).
- [49] G. Catalan, L. J. Sinnamon, and J. M. Gregg, *J. Phys.: Condens. Matter* **16**, 2253 (2004).
- [50] I. Naumov, A. M. Bratkovsky, and V. Ranjan, *Phys. Rev. Lett.* **102**, 217601 (2009).
- [51] Q. Deng, L. Liu, and P. Sharma, *J. Mech. Phys. Solids* **62**, 209 (2014).
- [52] Q. Deng, L. Liu, and P. Sharma, *Phys. Rev. E* **90**, 012603 (2014).
- [53] A. Livne, E. Bouchbinder, and J. Fineberg, *Phys. Rev. Lett.* **101**, 264301 (2008).